Emergent Dynamic Instability in Micrometre-scale Synthetic Active-matter Polymers

Yonatan Biniuri[1]*, Maria Bespalova[1], Philippe I.H. Bastiaens[1]

1. Department of Systemic Cell Biology, Max Planck Institute of Molecular Physiology, Dortmund, Germany

Corresponding Author

Correspondence to Yonatan Biniuri (Yonatan.biniuri@mpi-dortmund.mpg.de)

Supplementary information

Table S1. Monomer DNA and DNA/RNA strands used in this work

Name	Sequence (5′-3′)	Length
Sc		
Sc1	CGTATTGGACATTTCCGTAGACCGACTGGACATCTTC	37
Sc3	TCTACGGAAATGTGGCAGAATCAATCATAAGACACCAGTCGG	42
Sc3F	/5Alex488N/ TCTACGGAAATGTGGCAGAATCAATCATAAGACACCAGTCGG	42
Sc2	CCTCACCTTCACACCAATACGAGGTA	26
Sc2Polar	CCTCACCTTCACACCAATACGGCATT	26
Sc4	CAGACGAAGATGTGGTAGTGGAATGC	26
Sc5	CCACTACCTGTCTTATGATTGATTCTGCCTGTGAAGG	37
Cat		
Cat1	CTCAGTGGACAGCCGTTCTGGAGCGTTGGACGAAACT	37
Cat2	GTCTGGTAGAGCACCACTGAGGCATT	26
Cat2Polar	GTCTGGTAGAGCACCACTGAGAGGTA	26
Cat3	CCAGAACGGCTGTGGCTAAACAGTAACCGAAGCACCAACGCT	42
Cat3F Overhang	CCAGAACGGCTGTGGCTAAACAGTAACCGAAGCACCAACGCT GGTAAGTCTCCTTCTTATCT	62
Cat3 Overhang	TCCTCCTCCTCCTCCTCCTCCTCCTCCTCCTCCTCCTCCTCCTCCTCTTA GATAAGAAGGAGACTTACC	
Cat4	TGAGGAGTTTCGTGGTCATCGTACCT	26
Cat5	CGATGACCTGCTTCGGTTACTGTTTAGCCTGCTCTAC	37
Cat5 SubComp	CGATGACCTGCTTCGGTTACTGTTTAGCCTGATCTAC	37
Cat2-mockSub	CTGGTCTGGTAGATCACCACTGAGGCATT	29
Cat2-Sub2R-Polar	CTGGTCTGGTArGrATCACCACTGAGAGGTA	31
Cat2-mockSub-Polar	CTGGTCTGGTAGATCACCACTGAGAGGTA	29
Cat2-Sub3R-Polar	CTGGTCTGGTArGrArUCACCACTGAGAGGTA	29
Cat2-Sub2R	CTGGTCTGGTAGrArUCACCACTGAGGCATT	29

Cat2-Sub3R	CTGGTCTGGTArGrArUCACCACTGAGGCATT	29
Catalyst		
DzI	CTC AGT GGT GA GGCTAGCTACAACGA CTAC CAG ACC AG	38
DzI +T	CTC AGT GGT GA GGCTAGCTACAACGA TCTAC CAG ACC AG	39
DzII	AGT GGT GA GGCTAGCTACAACGA CTAC CAG ACC AG	35
DzIII	CTC AGT GGT GA GGCTAGCTACAACGA CTAC CAG AC	35
DzIV	AGT GGT GA GGCTAGCTACAACGA CTAC CAG AC	32
iDz	CGCACCCA GGCTAGCTACAACGA CTCTCTCC	31
Mut	CTCAGTGGTGA AGTCGGATCGACCAA CTACCAGACCAG	40
Coupler		
CpI	AGATAAGAAGGAGACTTACCTTAGATAAGAAGGAGACTTACC	42
CpIDbl	GATAAGAAGGAGACTTACCTTTTGATAAGAAGGAGACTTACCTTTTGATAAGAAGG AGACTTACCTTTTGATAAGAAGGAGACTTACC	88

Table S2. Substrate RNA insertion sequences

RNA substrate sequence	Strand sequence (5'-3')	Catalytic activity
rG	/5ATTO647NN/CTGGTCTGGTA**rG**AUCACCACTGAGAGGTA	-
rA	/5ATTO647NN/CTGGTCTGGTArG**rA**UCACCACTGAGAGGTA	-
rGrA	/5ATTO647NN/CTGGTCTGGTA**rGrA**UCACCACTGAGAGGTA	-
rArU	/5ATTO647NN/CTGGTCTGGTAG**rArU**CACCACTGAGAGGTA	+
rGrArU	/5ATTO647NN/CTGGTCTGGTA**rGrArU**CACCACTGAGAGGTA	+

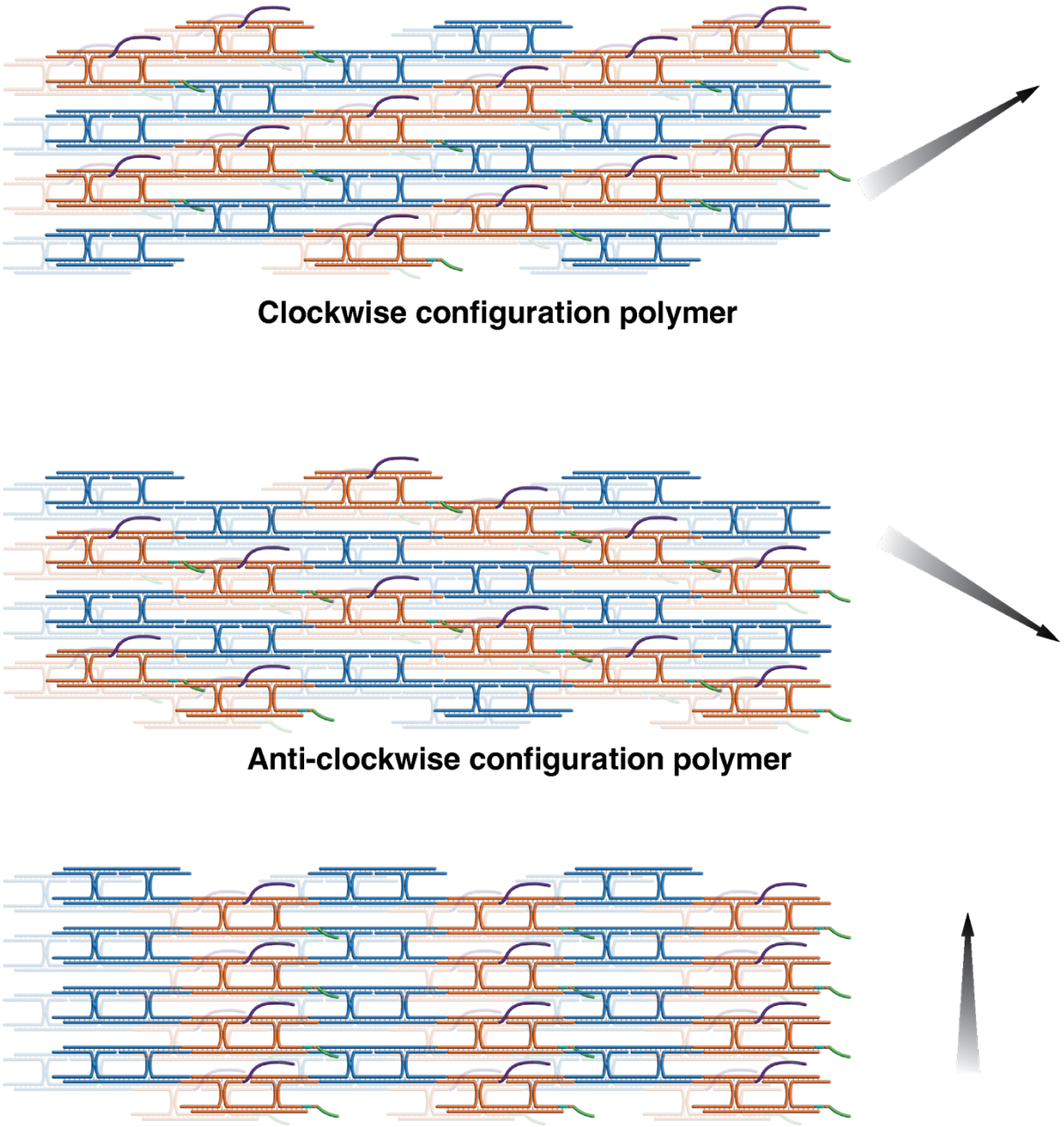

Figure S1a. Different spatial polymer-filament configuration assessed

Different, spatial, two-monomer, polymer configurations assessed at different stages of this work. Configuration (i) shows the two monomer variants assembling into a clock wise pattern containing polymer. This polymer variant is the one that was used for the described assays and experiments described in this work. Configuration (ii) also shows a diagonal forming symmetry, but at an anti-clock-wise pattern. Configuration (iii) was composed of the banded assembly of the two monomer variants, but was deemed too fragile for the dissipative and non-equilibrium properties we sought to demonstrate, due to its striped configuration, resulting in many break facets along the polymer's length.

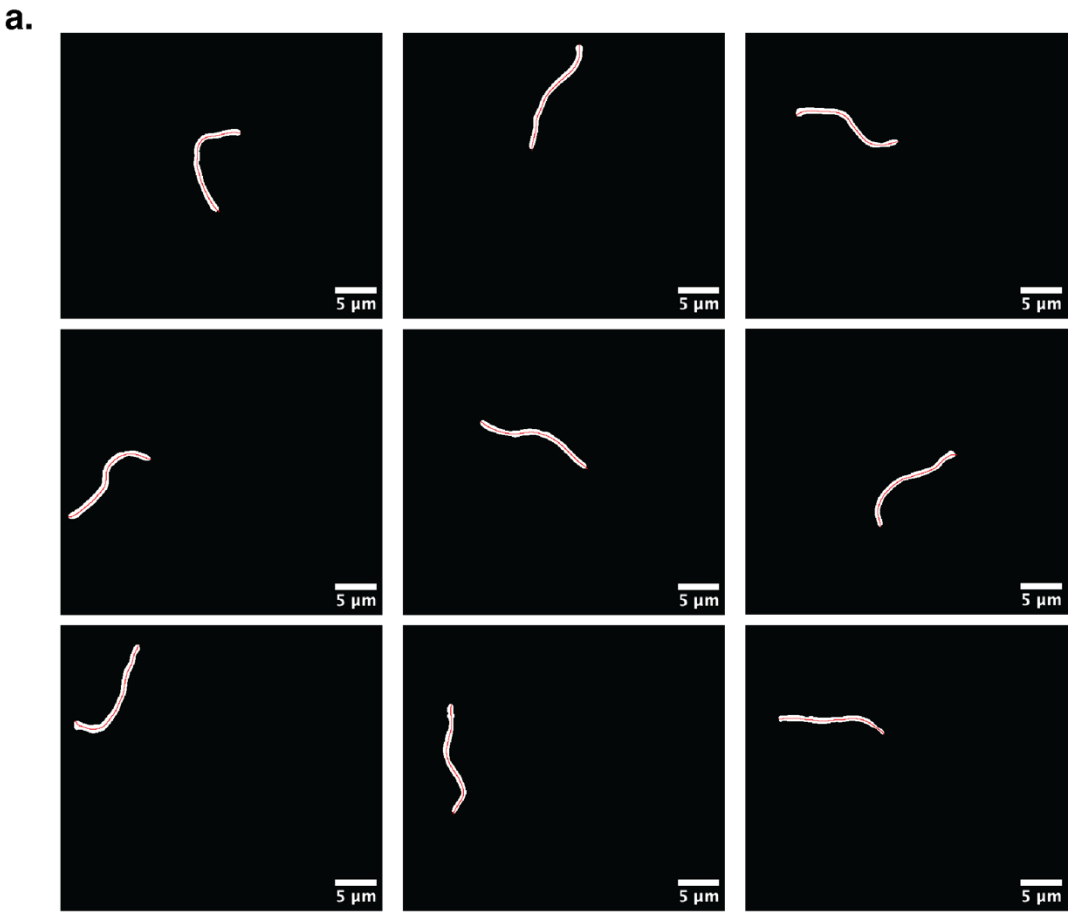

Figure S1b. Measuring the persistence length of the hybrid DNA/RNA polymers
a. Representative configurations of a freely diffusing DNA/RNA hybrid filament used to assess the dissipative filaments' persistence length. A 400 nM MMCat/MMSc mixture was loaded onto a passivated slip and glass slide sandwich, resulting in a 1.5 – 2.2 µm thick, dimensionally reduced confinement for the filaments, and loaded onto a 35 °C, heated, sealed microscope sample holder, and let polymerize for ca. 15

minutes. Upon reaching equilibrium, Individual filaments were recorded at 0.16 second intervals for 100 frames to capture a wide array of possible filament spatial-configurations. Filaments were then processed using Fiji's tubeness algorithm, with half the apparent filament cross-section width value (0.2) used as the sigma value, followed by a masking and binarizing step. Individual filaments coordinates were then extracted using the ridge finder plugin in Fiji. We then measured the persistence length of the dissipative filaments as previously described[1,3]. Lengths of 2 μm < Δx< 9.5 μm were used for fitting the data using equation 1. The resulting persistence length was measured at 9.43 ± 1.83 μm.

1. $$< \hat{t}\,(x) \cdot \hat{t}\,(x + \Delta x >) = e^{-\frac{\Delta x}{2P}}$$

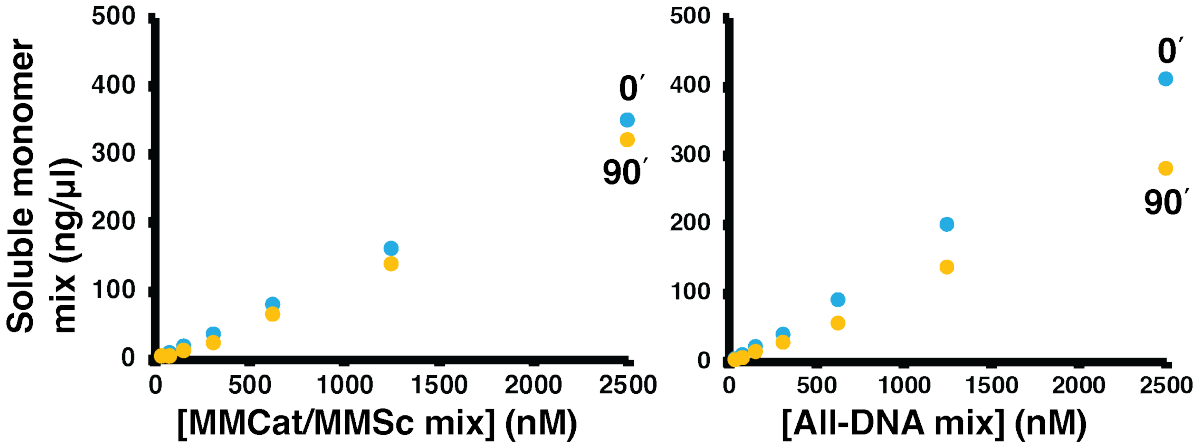

Figure S1c. Polymerizing fraction at different concentrations and critical concentration determination

Polymer fraction as a function of the available free monomer concentration for the all-DNA control system, and the DNA/RNA hybrid system. Each graph depicts two time points 0' and 90', demonstrating the progress of the polymerization process and the transition of a larger fraction of the free, soluble, monomer into the polymerized filament state. The DNA/RNA hybrid system showed an overall lower yield of polymer forming, due to its dissipative properties resulting in constant cleavage and depolymerization of the forming polymer. The critical concentration, the concentration in which no detectable polymer growth was observed, was determined at 40 nM for the DNA/RNA hybrid system, and 35 nM for the all-DNA system.

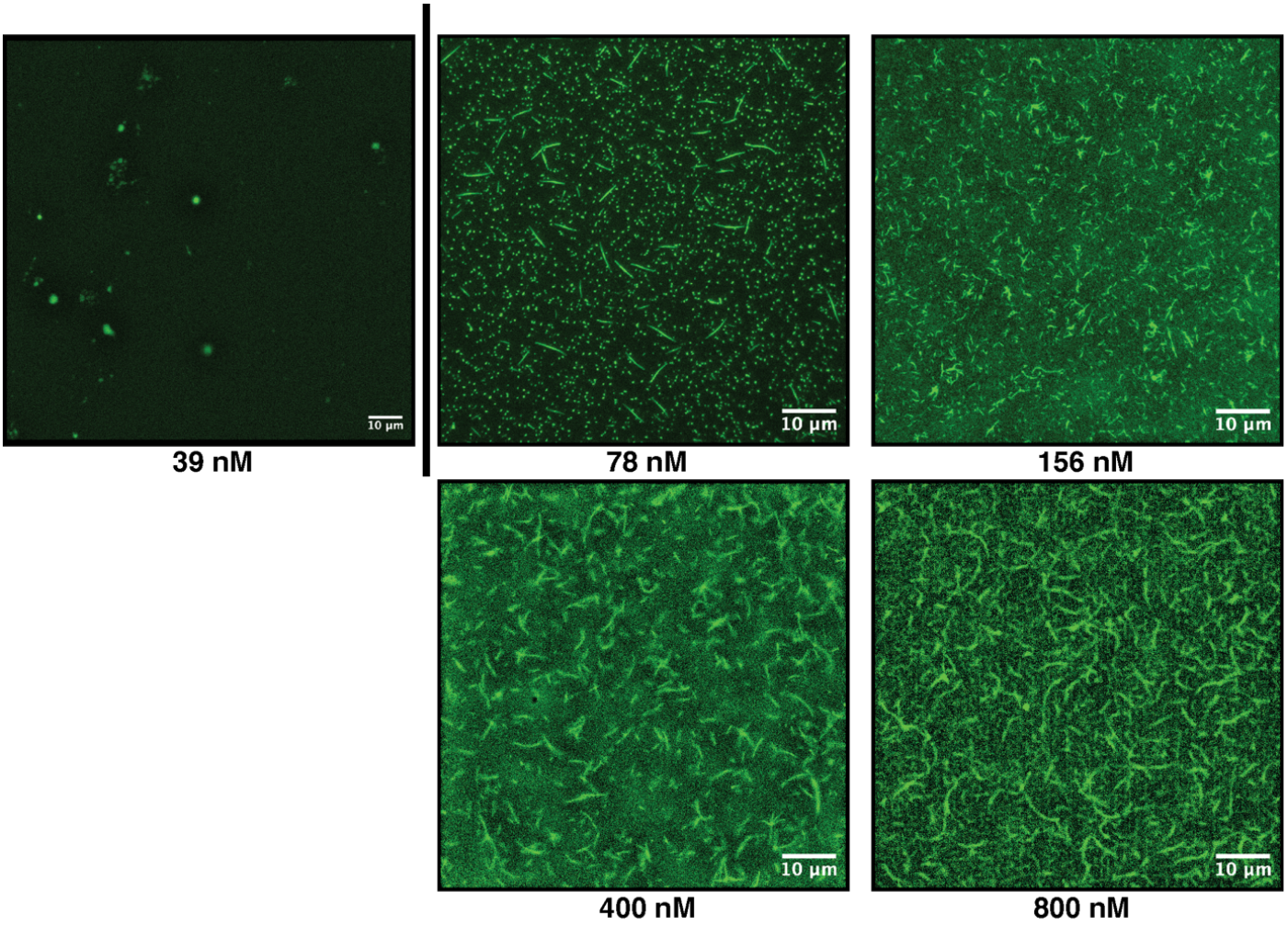

Figure S1d. Microscopy images of the DNA/RNA-hybrid monomer-units at different monomer concentrations

Representative epifluorescence microscopy images of the DNA/RNA hybrid system at different free monomer concentration. The perpendicular black line represents the critical concentration threshold. The MMCat/MMSc monomer was mixed in 1xTAE-Mg^{2+} buffer, and was let to polymerize in a test tube at 35 °C for 10'. For each of the different concentrations, a volume of 1 µl of the reaction mixture was loaded onto a new, raw glass slip and slide sandwich, and imaged using the 488 nm channel.

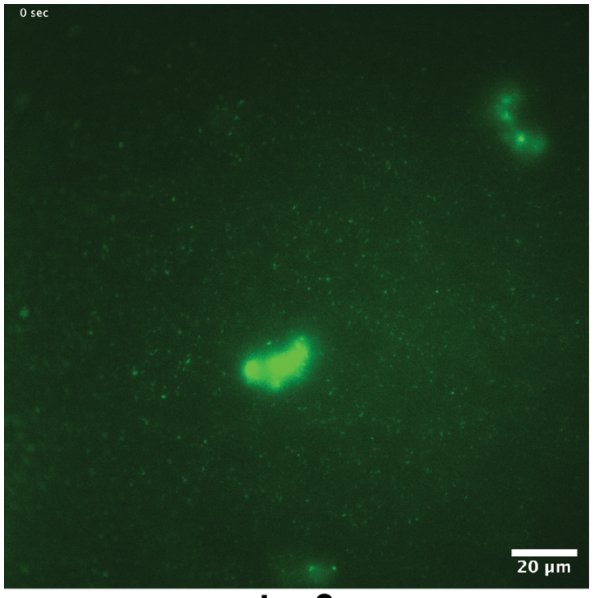

t = 0

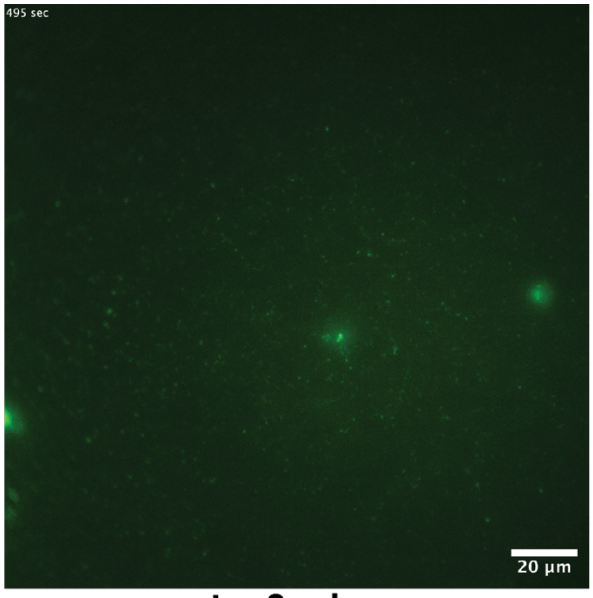

t = 8 mins

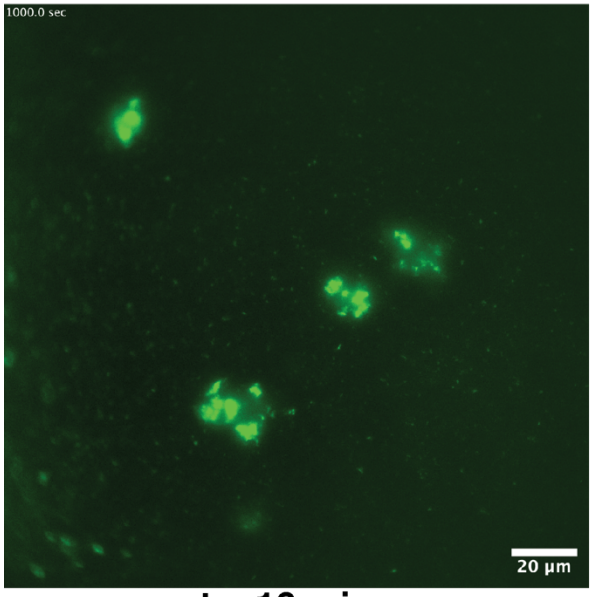

t = 16 mins

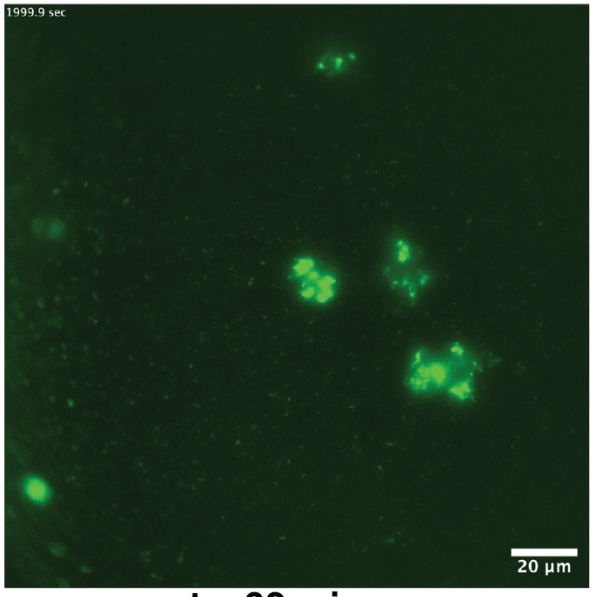

t = 32 mins

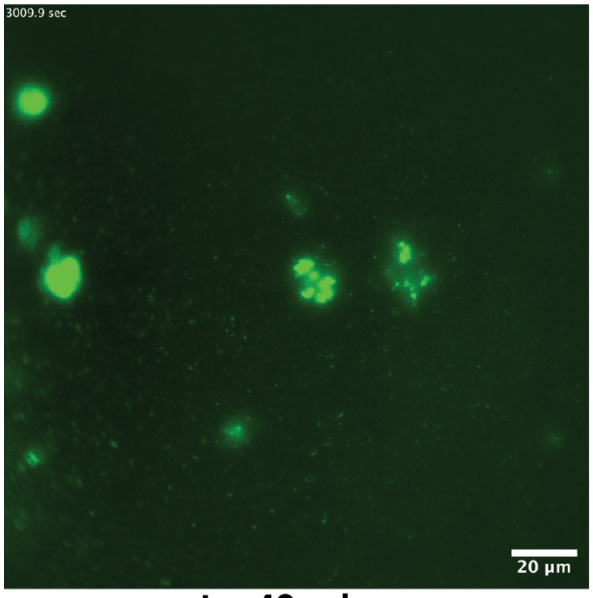

t = 49 mins

Figure S2a. DNA/RNA hybrid monomer-units polymerization at 23 °C

Epifluorescence microscopy images of the DNA/RNA hybrid system polymerization assay performed at 23 °C. 200 nM MMCat/MMSc monomer mixture in 1xTAE-Mg^{2+} buffer was loaded onto a passivated glass slip and slide sandwich, which was sealed using a two-component dental silicone compound, to avoid the sample evaporating. The polymerization assay at 23 °C resulted in the formation of blobby aggregates, instead of the ordered filaments forming under higher temperature regimes.

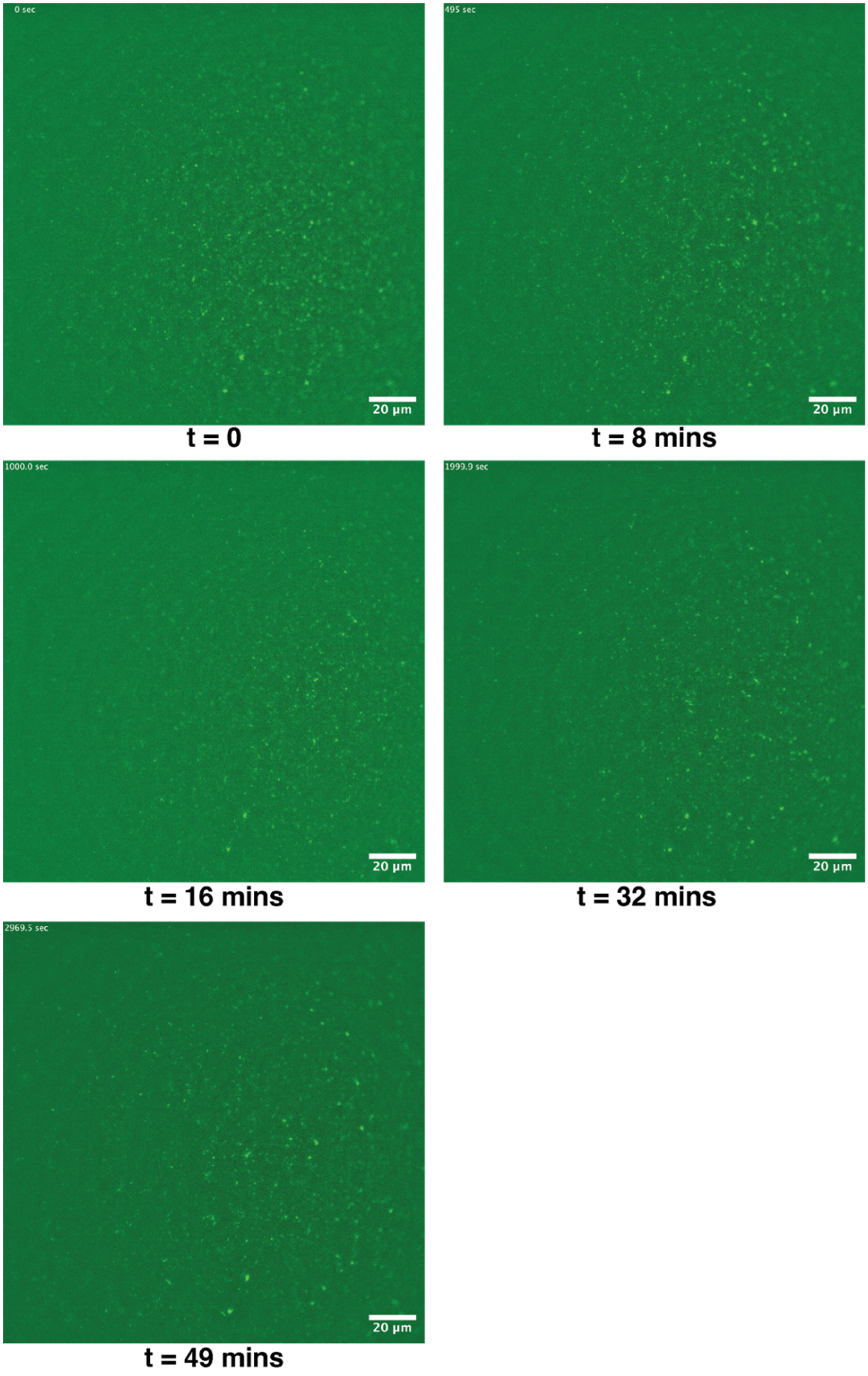

Figure S2b. All-DNA monomer-units polymerization at 23 °C

Epifluorescence microscopy images of the all-DNA system polymerization assay performed at 23 °C. 200 nM all-DNA monomer mixture in 1xTAE-Mg^{2+} buffer was

loaded onto a passivated glass slip and slide sandwich, which was sealed using a two-component dental silicone compound, to avoid the sample evaporating. The polymerization assay at 23 °C resulted in the slow formation of few short polymer filaments over ca. 60 minutes, instead of the longer filaments which started polymerizing nearly instantly under higher temperature regimes.

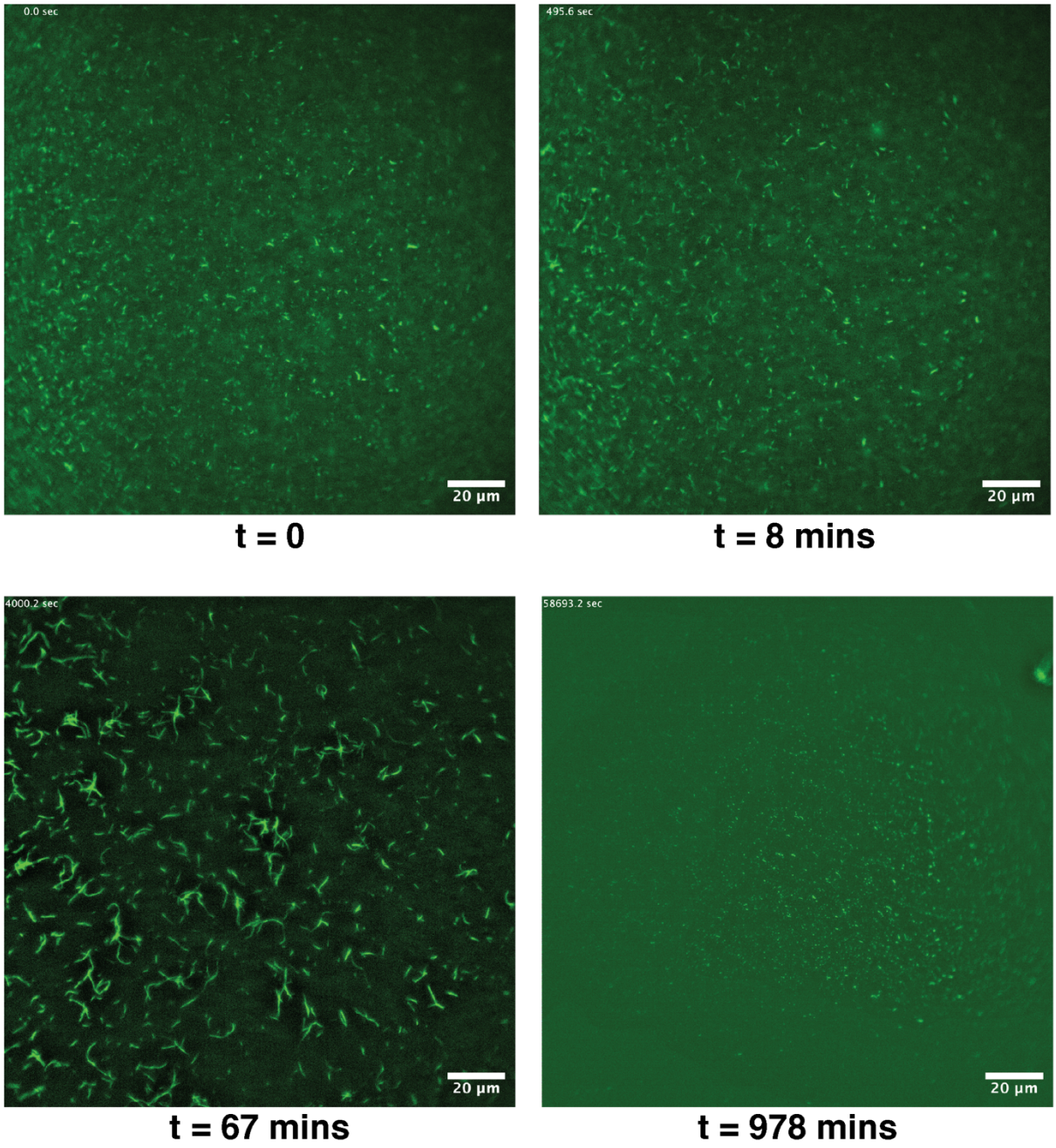

Figure S3. DNA/RNA hybrid monomer-units overnight polymerization and degradation at 35 °C

Epifluorescence microscopy images of the DNA/RNA hybrid system polymerization assay performed at 35 °C. 200 nM MMCat/MMSc monomer mixture in 1xTAE-Mg^{2+} buffer was loaded onto a passivated glass slip and slide sandwich, which was sealed using a two-component dental silicone compound, to avoid the sample evaporating. The polymerization assay at 35 °C resulted in the formation of long, smooth polymer filaments, which demonstrated some cleaving events along the polymerization phase. After ca. 100 mins, no filaments were observed, indicating the depletion of the MMCat monomer due to its intrinsic RNA-cleavage properties.

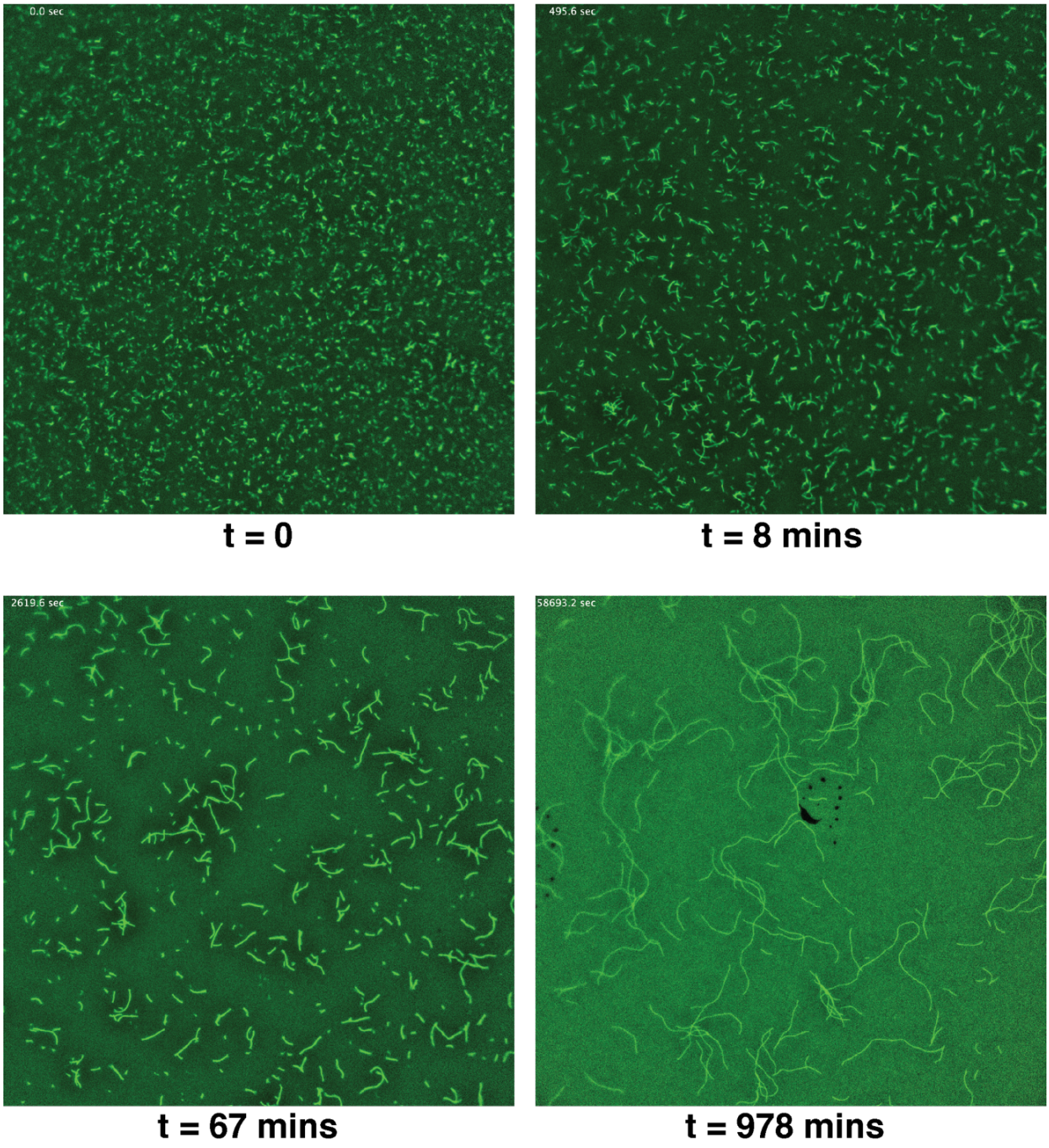

Figure S4. All-DNA monomer-units overnight polymerization at 35 °C

Epifluorescence microscopy images of the all-DNA hybrid system polymerization assay performed at 35 °C. 200 nM all-DNA monomer mixture in 1xTAE-Mg^{2+} buffer was loaded onto a passivated glass slip and slide sandwich, which was sealed using a two-component dental silicone compound, to avoid the sample evaporating. The polymerization assay at 35 °C resulted in the formation of long, smooth polymer filaments, which when let incubate for ca. 16 hours resulted in very long (40 µm), smooth filaments. It should be noted that these filaments did not exhibit any cleaving events along the filament structure. Filaments appeared stable when stable was imaged a second after 90 days (not shown).

All-DNA

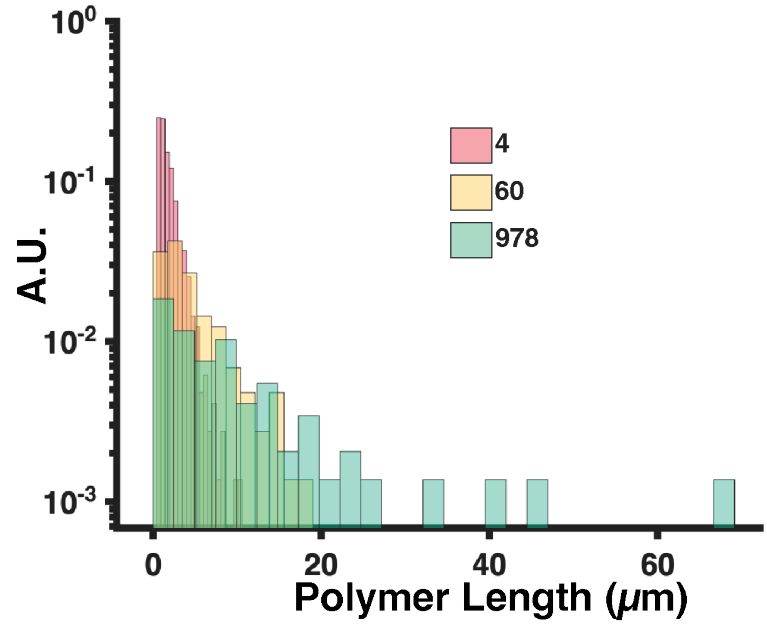

DNA/RNA hybrid

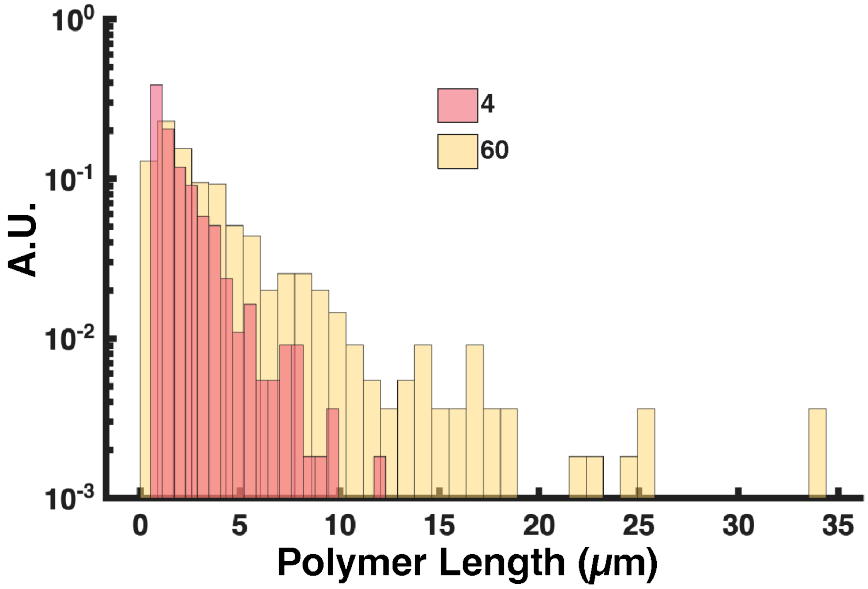

Figure S5. Time-dependent evolution of filament length distribution
Change in filament length distribution of the all-DNA and DNA/RNA hybrid systems over time. DNA/RNA hybrid polymers completely depolymerized at 978 minutes.

a.

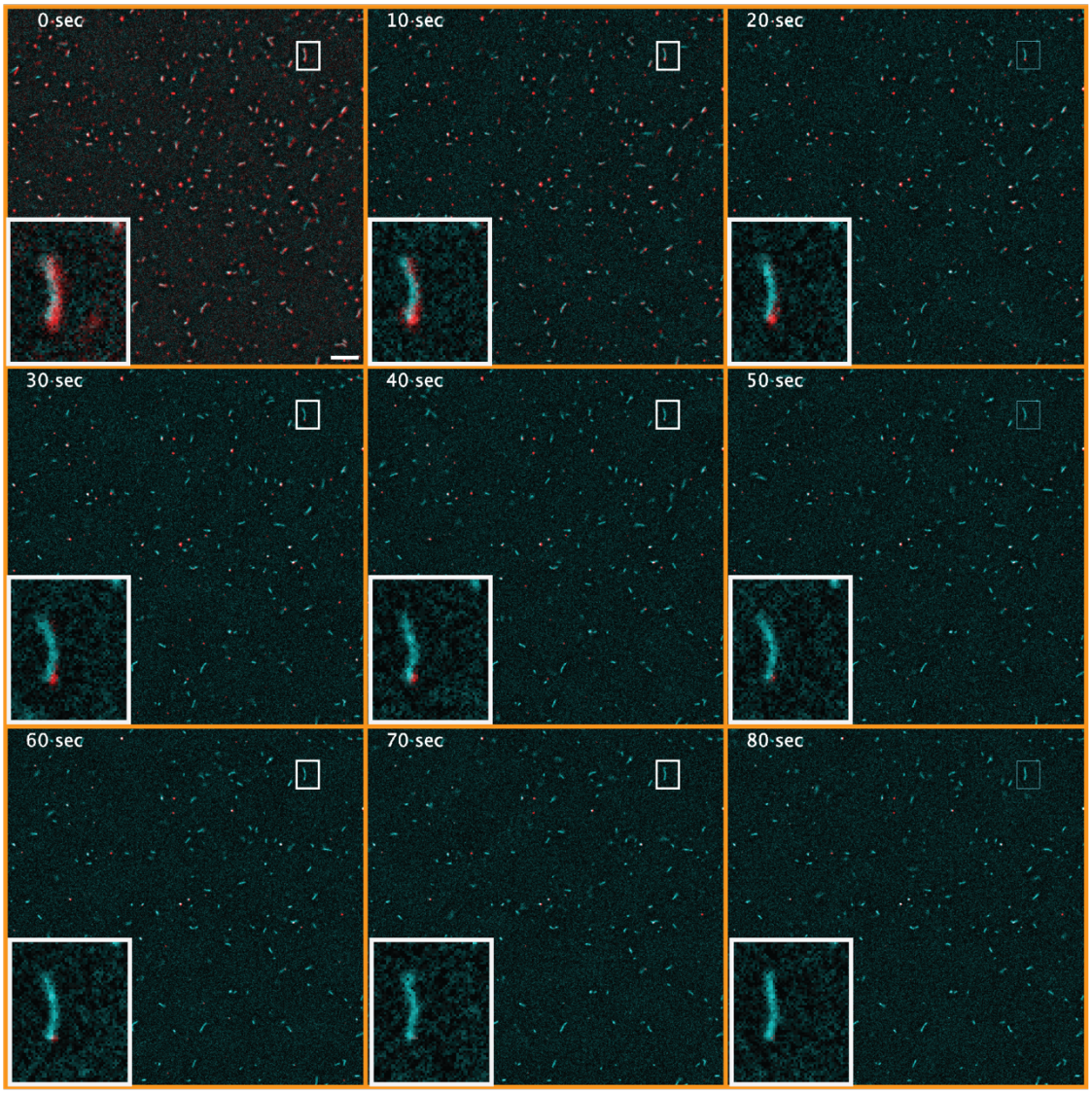
0 sec
10 sec
20 sec
30 sec
40 sec
50 sec
60 sec
70 sec
80 sec

b.

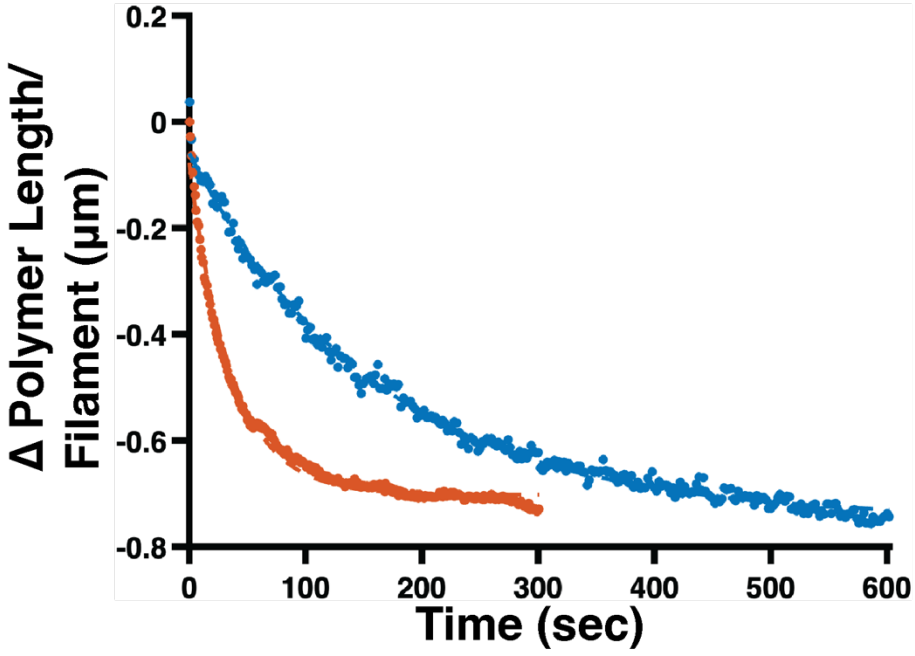
Δ Polymer Length/
Filament (μm)
0.2
0
-0.2
-0.4
-0.6
-0.8
0
100
200
300
400
500
600
Time (sec)

Figure S6. Decrease of 640nm RNA Marker compared with the 488nm scaffold marker

Image time series depicting the time-dependent decrease in the fluorescence-signal intensity for the Alexa488-labelled MMSc monomer and the intrinsically cleaving Atto647-labelled MMCat as a result of filament depolymerization. The Atto647 fluorescent label was located downstream of the RNA-cleavage site, resulting in the loss of the fluorescent signal upon the slow, spontaneous or, fast, DNAzyme-mediated cleavage of the RNA bases within MMCat. Under depleted free-monomer conditions, the Atto647 decreases more rapidly when compared with the MMSc's, non-cleaving, Alexa488 fluorescent label. Filament depolymerization, under these conditions, is followed within tens of seconds. Time dependent decrease in apparent polymer length per filament for the MMSc-Alexa488 label and MMCat-Atto647 label. The fluorescence signal was normalized using the bleaching curve of the polymer-attached dye in the absence of the DNAzyme catalyst.

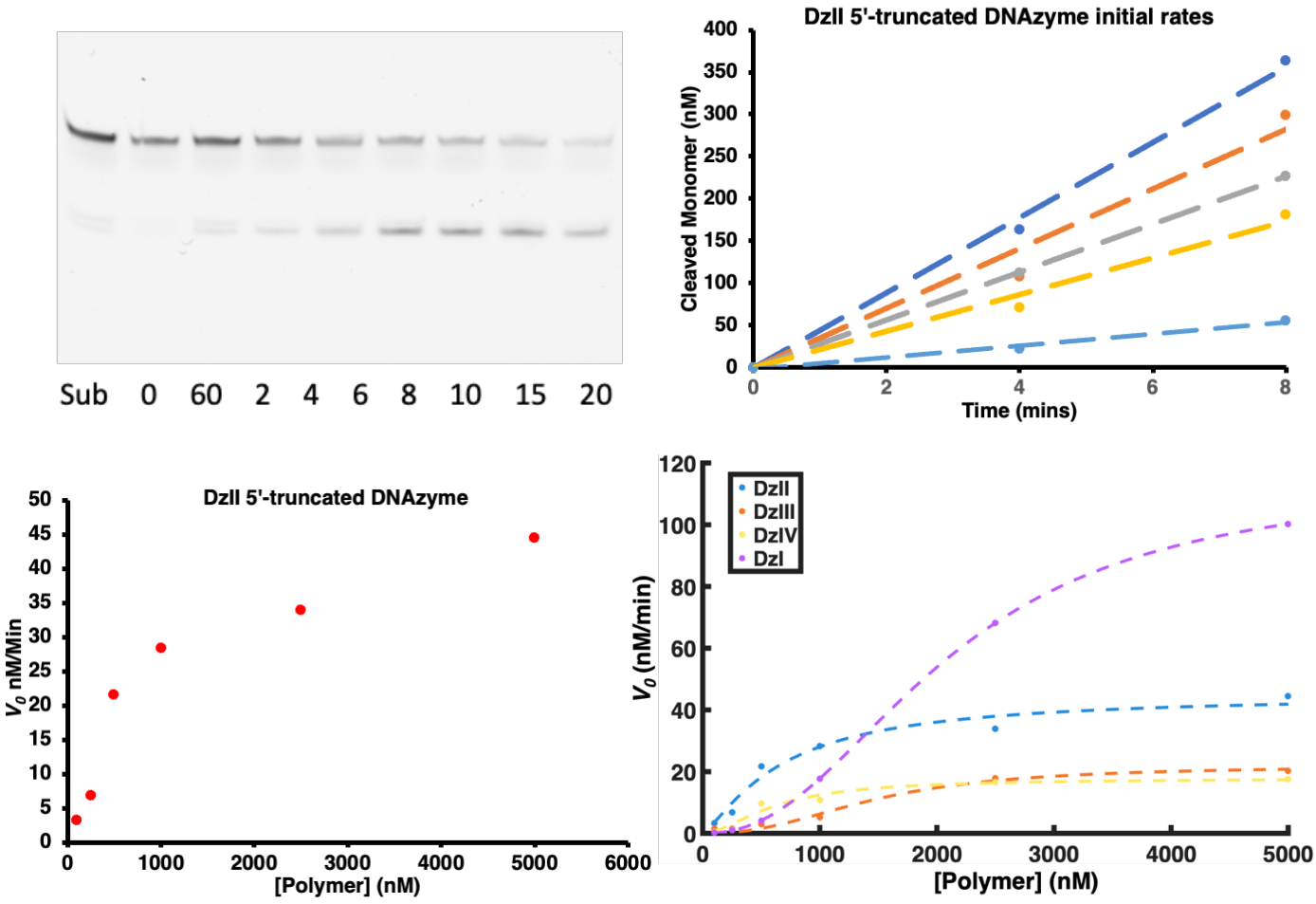

Figure S7. Extraction and calculation of the Michaelis-Menten kinetic parameters for the different Dz variants

Representative work flow for the extraction of the Michaelis-Menten kinetic parameters for the different DNAzyme variants and the DNA/RNA hybrid system acting as substrate. Seven different DNA/RNA hybrid polymer concentrations were mixed with the different DNAzyme variants (I, II, III, and IV) under saturation conditions, moved onto a covered heating block set at 35 °C, aliquots removed onto ice-cold stop buffer at the desired time points, and mixed 1:1 v/v with 1x Novex™ TBE-Urea Sample Buffer (0.5x final buffer concentration). Aliquots were then diluted accordingly to ensure detection of signal across all time points, and loaded onto a urea-PA gel. Initial kinetic rates were then plotted for each of the different polymer concentrations, and plotted a second time as a function of the polymer concentration used, resulting in Michaelis-Menten plots for each of the DNAzyme-catalyst variants, and their corresponding kinetic parameters.

Table S3. Michaelis-Menten kinetics values for the different Dz variants

Catalyst variant	V_{max} (nM/min)	K_m (nM)	$k_{cat} * 10^1$ (min^{-1})
DzI	114.2±10.2	2103±105.0	0.11
DzII	45.1±6.2	678.3±83.2	0.05
DzIII	21.9±4.1	1471±159.0	0.02
DzIV	17.8±4.3	618.5±146.2	0.02

Table S4. Substrate toehold variants and their spatial representations

Toehold(TH) length	Strand sequence (5'-3')	Polymer formation
3	/5ATTO647NN/**CTG**GTCTGGTAGrArUCACCACTGAGAGGTA	+
6	/5ATTO647NN/**GGACTG**GTCTGGTAGrArUCACCACTGAGAGGTA	+
9	/5ATTO647NN/**CACGGACTG**CTGGTCTGGTAGrArUCACCACTGAGAGGTA	-

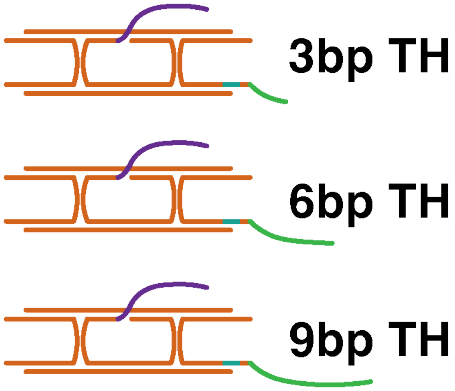

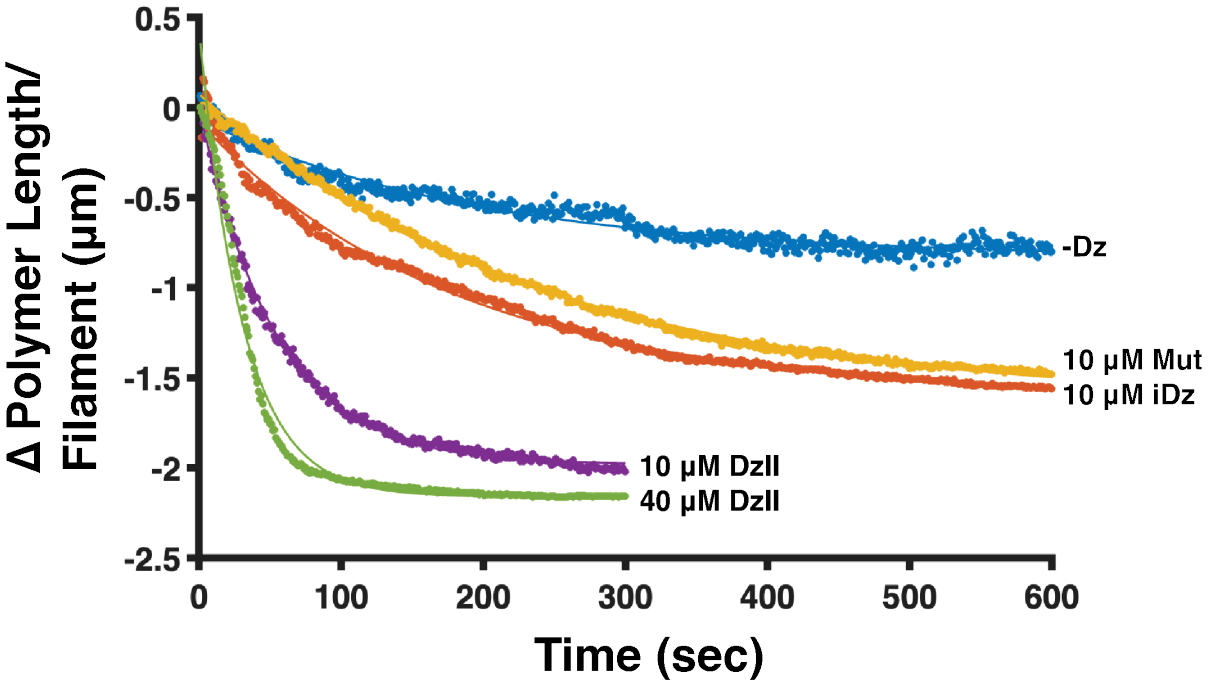

Figure S8. Time dependent change in polymer filament length per filament as a function of the introduction of different catalysts and controls

(-Dz) corresponds to the presence of no catalyst, (Mut) The addition of 10 μM of the randomly-mixed DNAzyme catalytic core with complementary binding domains, (iDz) The addition of 10 μM of the iDz DNAzyme variant, which contained an active catalytic core, but mismatched binding domains, (DzII) The addition of either 10 μM or 40 μM of the DNAzyme variant DzII.

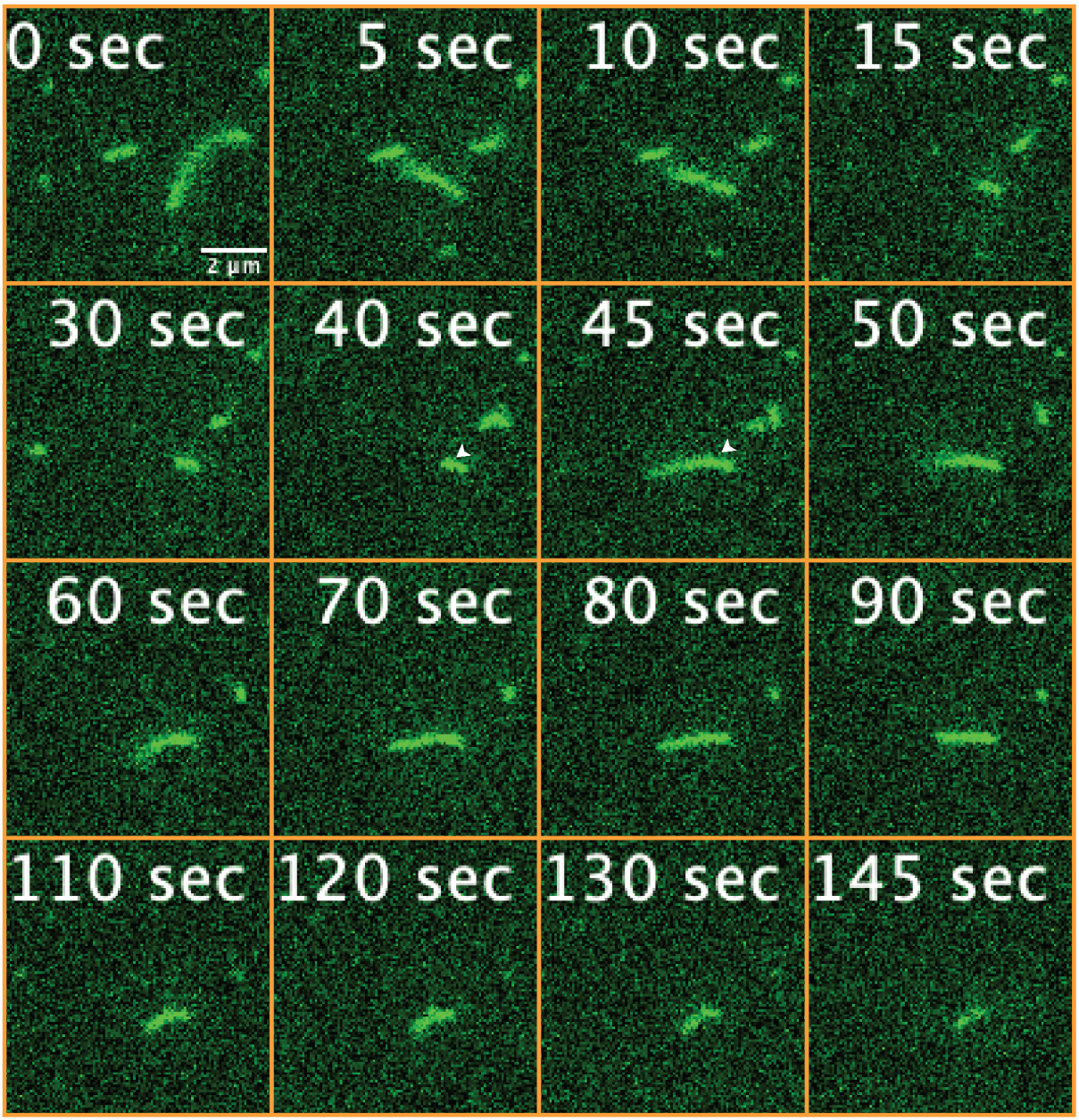

Figure S9. Polymer recovery event under downhill reaction conditions
A solution containing 0.4 µM MMCat/MMSc,1.2 µM DzII and 2mg/ml BSA was mixed in 1xTAE-Mg^{2+} buffer, pipetted onto passivated glass slip-sandwich, and sealed using two-component silicone to avoid evaporation. Imaging was performed using an Epifluorescent microscope equipped with a humidity regulated, heated box at 35 °C. White arrows in the images time series point to a recovery event.

Table S5.

Origami seed strands used in this work

Seed Group	Sequence
Template	M13mp18(7249 bases)
T5R2E_HP	ACAAACAACTGCCTATCACGACGCTTTTGCGTCGTGTTTTCGGAACCTGAGACT
T5R4E_HP	TCGGCATTCCGCCGCCGTCGCTGCTTTTGCAGCGACTTAGCATTGATGATATTC
T5R6E_HP	ATTGAGGGAATCAGTACGGAGCACTTTTGTGCTCCGTTGCGACAGACGTTTTCA
T5R8E_HP	GAAGGAAAAATAGAAAGCCTAGCGTTTTCGCTAGGCTTATTCATATTTCAACCG
T5R10E_HP	CTTTACAGTATCTTACCGCTCGTGTTTTCACGAGCGTTCGAAGCCCAGTTACCA
T5R12E_CYC_HP	CCTCAAGATCCCAATCCGTGGAGCTTTTGCTCCACGTTCAAATAAGATAGCAGC
T5R2F_HP	AATGCCCCATAAATCCGCTCGGACTTTTGTCCGAGCTTTCATTAAAAGAACCAC
T5R4F_HP	CACCAGAGTTCGGTCAGCCGAGCGTTTTCGCTCGGCTTTAGCCCCCTCGATAGC
T5R6F_HP	AGCACCGTAGGGAAGGTCGGAGGCTTTTGCCTCCGATTTAAATATTTTATTTTG
T5R8F_HP	TCACAATCCCGAGGAACTGGTGGCTTTTGCCACCAGTTACGCAATAATGAAATA
T5R10F_HP	GCAATAGCAGAGAATACCGCAGGCTTTTGCCTGCGGTTACATAAAAACAGCCAT
T5R12F_CYC_HP	ATTATTTAGAAGGATTGCCATCGCTTTTGCGATGGCTTAGGATTAGAAACAGTT
T3R2E_HP	GGAAAGCGGTAACAGTGTGGCAGCTTTTGCTGCCACTTGCCCGTATCGGGGTTT
T3R4E_HP	GTTTGCCACCTCAGAGACCAGGCGTTTTCGCCTGGTTTCCGCCACCGCCAGAAT
T3R6E_HP	TTATTCATGTCACCAAGCTCGCTGTTTTCAGCGAGCTTTGAAACCATTATTAGC
T3R8E_HP	ATACCCAAACACCACGCCTACCGCTTTTGCGGTAGGTTGAATAAGTGACGGAAA
T3R10E_HP	GCGCATTAATAAGAGCCTGGACGCTTTTGCGTCCAGTTAAGAAACAATAACGGA
T3R12E_CYC_HP	TGCTCAGTGCCAGTTAGGTGGTCGTTTTCGACCACCTTCAAAATAAACAGGGAA
T3R2F_HP	TGCCTTGACAGTCTCTGTCGGTGCTTTTGCACCGACTTGAATTTACCCCTCAGA
T3R4F_HP	GCCACCACTCTTTTCACGGTCGGCTTTTGCCGACCGTTTAATCAAATAGCAAGG
T3R6F_HP	CCGGAAACTAAAGGTGGACCTGGCTTTTGCCAGGTCTTAATTATCATAAAAGAA
T3R8F_HP	ACGCAAAGAAGAACTGTCGGCTCGTTTTCGAGCCGATTGCATGATTTGAGTTAA
T3R10F_HP	GCCCAATAGACGGGAGCACAGGCGTTTTCGCCTGTGTTAATTAACTTTCCAGAG
T3R12F_CYC_HP	CCTAATTTACCAGGCGTCGGAGCGTTTTCGCTCCGATTGATAAGTGGGGGTCAG
T1R2E_HP	TAAGCGTCGGTAATAACAGGAGCGTTTTCGCTCCTGTTGTTTTAACCCGTCGAG
T1R4E_HP	AACCAGAGACCCTCAGGCAGTCGCTTTTGCGACTGCTTAACCGCCACGTTCCAG
T1R6E_HP	GACTTGAGGTAGCACCGTCTGGCGTTTTCGCCAGACTTATTACCATATCACCGG
T1R8E_HP	TTATTACGTAAAGGTGTGGCTGCGTTTTCGCAGCCATTGCAACATACCGTCACC
T1R10E_HP	TGAACAAAGATAACCCAGTGCCTGTTTTCAGGCACTTTACAAGAATACGTCACC
T1R12E_CYC_HP	AGGGTTGAACGCTAACGCCAGGACTTTTGTCCTGGCTTGAGCGTCTGAACACCC
T1R2F_HP	AGTGTACTATACATGGCTCCTGCGTTTTCGCAGGAGTTCTTTTGATCTTTCCAG
T1R4F_HP	GAGCCGCCCCACCACCGTCAGGCGTTTTCGCCTGACTTGGAACCGCTGCGCCGA
T1R6F_HP	AATCACCACCATTTGGCGTCCTGCTTTTGCAGGACGTTGAATTAGACCAACCTA
T1R8F_HP	TACATACACAGTATGTCGGACCTGTTTTCAGGTCCGTTTAGCAAACTGTACAGA
T1R10F_HP	ATCAGAGAGTCAGAGGCGAGGTCGTTTTCGACCTCGTTGTAATTGAACCAGTCA
T_1R12F_CYC_HP	CCAAAATATACTCAGGTGCGGTCGTTTTCGACCGCATTAGGTTTAGATAGTTAG
Strand Name Sequence	
A1_AS1_RE_1	CAGCCAAGACGCAGGTAGCGAGACAGAGCTGAAAGTATTAAGAGG
A1_AS1_RE_3	TCGCTACCTGCGTTCGTCGGATGGTGAGGTCCACGCTCTGTC
A1_AS1_RE_5	CTATTATTCTGAAACAGTGGACCTCACCATCCGACGACACGAGCA
A1_AS2_SE_1	CACGGAGTCGAAGCGTAGGACGGTAGCCAGTCAGACGATTGGCCT
A1_AS2_SE_3	GTCCTACGCTTCGGACCTTGGTGATGCTGGACTGTGGCTACC
A1_AS2_SE_5	CAGGAGGTTGAGGCAGCAGTCCAGCATCACCAAGGTCGCTCGGCA
A1_AS3_RE_1	CAGCCAAGCGGCATGGTCTTGCGTTGGAGGCGTCAGACTGTAGCG
A1_AS3_RE_3	CAAGACCATGCCGACCTCATCCTCGCTTTCGGTGCTCCAACG
A1_AS3_RE_5	ATCAAGTTTGCCTTTACACCGAAAGCGAGGATGAGGTCACGAGCA
A1_AS4_SE_1	CACGGAGTCTACGGCAGTGACCGATCTCCAGACAAAAGGGCGACA
A1_AS4_SE_3	GTCACTGCCGTAGCTCACGAGGCACAACCACAGCGGAGATCG
A1_AS4_SE_5	GGTTTACCAGCGCCAAGCTGTGGTTGTGCCTCGTGAGGCTCGGCA
A1_AS5_RE_1	CAGCCAAGGTTCCACAGGACTCGCACTTCGCAGATAGCCGAACAA
A1_AS5_RE_3	AGTCCTGTGGAACACCACGAGACGCCATCGAGCGGAAGTGCG
A1_AS5_RE_5	TTTTTAAGAAAAGTAACGCTCGATGGCGTCTCGTGGTCACGAGCA
A1_AS6_SE_1	CACGGAGTCAAGGCTACGAGTCAGACAGGAACGTCAAAAATGAAA
A1_AS6_SE_3	ACTCGTAGCCTTGGACCGCACTCACCACTGCTCGCCTGTCTG
A1_AS6_SE_5	AAACGATTTTTTGTTTCGAGCAGTGGTGAGTGCGGTCGCTCGGCA
Fluorophores	
Unused_m13mp18_01	AAATTCTTACCAGTATAAAGCCAACTTTTGAGATCCGACTACGC
Unused_m13mp18_02	GCCTGTTTAGTATCATATGCGTTATTTTTGAGATCCGACTACGC
Unused_m13mp18_03	ACACCGGAATCATAATTACTAGAAATTTTGAGATCCGACTACGC
Unused_m13mp18_04	GATAAATAAGGCGTTAAATAAGAATTTTTGAGATCCGACTACGC
Unused_m13mp18_05	TTTAATGGTTTGAAATACCGACCGTTTTTGAGATCCGACTACGC
Unused_m13mp18_06	TTAGTTAATTTCATCTTCTGACCTATTTTGAGATCCGACTACGC

Unused_m13mp18_07	ACGCGAGAAAACTTTTTCAAATATATTTTGAGATCCGACTACGC
Unused_m13mp18_08	GATGCAAATCCAATCGCAAGACAAATTTTGAGATCCGACTACGC
Unused_m13mp18_09	TGGGTTATATAACTATATGTAAATGTTTTGAGATCCGACTACGC
Unused_m13mp18_10	ACTACCTTTTTAACCTCCGGCTTAGTTTTGAGATCCGACTACGC
Unused_m13mp18_11	AATTTATCAAAATCATAGGTCTGAGTTTTGAGATCCGACTACGC
Unused_m13mp18_12	TTAAGACGCTGAGAAGAGTCAATAGTTTTGAGATCCGACTACGC
Unused_m13mp18_13	TCCTTGAAAACATAGCGATAGCTTATTTTGAGATCCGACTACGC
Unused_m13mp18_14	TCGCTATTAATTAATTTTCCCTTAGTTTTGAGATCCGACTACGC
Unused_m13mp18_15	AGTGAATAACCTTGCTTCTGTAAATTTTTGAGATCCGACTACGC
Unused_m13mp18_16	GAAACAGTACATAAATCAATATATGTTTTGAGATCCGACTACGC
Unused_m13mp18_17	ATTTCATTTGAATTACCTTTTTTAATTTTGAGATCCGACTACGC
Unused_m13mp18_18	AGAAAACAAAATTAATTACATTTAATTTTGAGATCCGACTACGC
Unused_m13mp18_19	CAAAAGAAGATGATGAAACAAACATTTTTGAGATCCGACTACGC
Unused_m13mp18_20	GCGAATTATTCATTTCAATTACCTGTTTTGAGATCCGACTACGC
Unused_m13mp18_21	AATACCAAGTTACAAAATCGCGCAGTTTTGAGATCCGACTACGC
Unused_m13mp18_22	CAATAACGGATTCGCCTGATTGCTTTTTTGAGATCCGACTACGC
Unused_m13mp18_23	TAACAGTACCTTTTACATCGGGAGATTTTGAGATCCGACTACGC
Unused_m13mp18_24	CAGGTTTAACGTCAGATGAATATACTTTTGAGATCCGACTACGC
Unused_m13mp18_25	CAGAAATAAAGAAATTGCGTAGATTTTTTGAGATCCGACTACGC
Unused_m13mp18_26	CCATATCAAAATTATTTGCACGTAATTTTGAGATCCGACTACGC
Unused_m13mp18_27	TCTGAATAATGGAAGGGTTAGAACCTTTTGAGATCCGACTACGC
Unused_m13mp18_28	TATAATCCTGATTGTTTGGATTATATTTTGAGATCCGACTACGC
Unused_m13mp18_29	GATTATCAGATGATGGCAATTCATCTTTTGAGATCCGACTACGC
Unused_m13mp18_30	AAGGAGCGGAATTATCATCATATTCTTTTGAGATCCGACTACGC
Unused_m13mp18_31	CATTTTGCGGAACAAAGAAACCACCTTTTGAGATCCGACTACGC
Unused_m13mp18_32	TAATTTTAAAAGTTTGAGTAACATTTTTTGAGATCCGACTACGC
Unused_m13mp18_33	GTATTAAATCCTTTGCCCGAACGTTTTTTGAGATCCGACTACGC
Unused_m13mp18_34	TAGACTTTACAAACAATTCGACAACTTTTGAGATCCGACTACGC
Unused_m13mp18_35	ATAATACATTTGAGGATTTAGAAGTTTTTGAGATCCGACTACGC
Unused_m13mp18_66	AAACCGTCTATCAGGGCGATGGCCCTTTTGAGATCCGACTACGC
Unused_m13mp18_67	ACGTGGACTCCAACGTCAAAGGGCGTTTTGAGATCCGACTACGC
Unused_m13mp18_68	TTTGGAACAAGAGTCCACTATTAAATTTTGAGATCCGACTACGC
Unused_m13mp18_69	CCGAGATAGGGTTGAGTGTTGTTCCTTTTGAGATCCGACTACGC
Unused_m13mp18_70	AAATCCCTTATAAATCAAAAGAATATTTTGAGATCCGACTACGC
Unused_m13mp18_71	TGTTTGATGGTGGTTCCGAAATCGGTTTTGAGATCCGACTACGC
Unused_m13mp18_72	CTGGTTTGCCCCAGCAGGCGAAAATTTTTGAGATCCGACTACGC
Unused_m13mp18_73	TGAGAGAGTTGCAGCAAGCGGTCCATTTTGAGATCCGACTACGC
Unused_m13mp18_74	AGCTGATTGCCCTTCACCGCCTGGCTTTTGAGATCCGACTACGC
Unused_m13mp18_75	TTTCTTTTCACCAGTGAGACGGGCATTTTGAGATCCGACTACGC
Unused_m13mp18_76	GTTTGCGTATTGGGCGCCAGGGTGGTTTTGAGATCCGACTACGC
Unused_m13mp18_77	GAATCGGCCAACGCGCGGGGAGAGGTTTTGAGATCCGACTACGC
Unused_m13mp18_78	GAAACCTGTCGTGCCAGCTGCATTATTTTGAGATCCGACTACGC
Unused_m13mp18_79	TGCGCTCACTGCCCGCTTTCCAGTCTTTTGAGATCCGACTACGC
Unused_m13mp18_80	GAGTGAGCTAACTCACATTAATTGCTTTTGAGATCCGACTACGC
Unused_m13mp18_87	ACGACGTTGTAAAACGACGGCCAGTTTTTGAGATCCGACTACGC
Polymer adapters	
A1_AS135_RE_2	CCTCA TGCTCGTGCTTGGCTG GCATT
A1_AS246_SE_2	GTCTG TGCCGAGCACTCCGTG AGGTA
Seed flurophore strand	
Seed FI imagerDirect	/5ATTO550N/AAGCGTAGTCGGATCTC
Biotin binding seed sequences	
Biotin tag	/5Biosg/AGGAGTGACGATGTG
BDC strand on unused_m13mp18_36	CAACTAATAGATTAGAGCCGTCAATTTTTCACATCGTCACTCCT
BDC strand on unused_m13mp18_37	TATCTAAAATATCTTTAGGAGCACTTTTTCACATCGTCACTCCT
BDC strand on unused_m13mp18_38	ACTGATAGCCCTAAAACATCGCCATTTTTCACATCGTCACTCCT
BDC strand on unused_m13mp18_39	GAATGGCTATTAGTCTTTAATGCGCTTTTCACATCGTCACTCCT
BDC strand on unused_m13mp18_40	AGAATACGTGGCACAGACAATATTTTTTTCACATCGTCACTCCT
BDC strand on unused_m13mp18_41	ATAGAACCCTTCTGACCTGAAAGCGTTTTCACATCGTCACTCCT
BDC strand on unused_m13mp18_42	ATAAAAGGGACATTCTGGCCAACAGTTTTCACATCGTCACTCCT
BDC strand on unused_m13mp18_43	GCAGATTCACCAGTCACACGACCAGTTTTCACATCGTCACTCCT

BDC strand on unused_m13mp18_44	ATCGTCTGAAATGGATTATTTACATTTTTCACATCGTCACTCCT
BDC strand on unused_m13mp18_45	ATGGAAATACCTACATTTTGACGCTTTTTCACATCGTCACTCCT
BDC strand on unused_m13mp18_46	CCAGCCATTGCAACAGGAAAAACGCTTTTCACATCGTCACTCCT
BDC strand on unused_m13mp18_47	CTGGTAATATCCAGAACAATATTACTTTTCACATCGTCACTCCT
BDC strand on unused_m13mp18_48	GTAGAAGAACTCAAACTATCGGCCTTTTTCACATCGTCACTCCT
BDC strand on unused_m13mp18_49	TGATTAGTAATAACATCACTTGCCTTTTTCACATCGTCACTCCT
BDC strand on unused_m13mp18_50	AAATTAACCGTTGTAGCAATACTTCTTTTCACATCGTCACTCCT
BDC strand on unused_m13mp18_51	CCGAGTAAAAGAGTCTGTCCATCACTTTTCACATCGTCACTCCT
BDC strand on unused_m13mp18_52	GAAGTGTTTTTATAATCAGTGAGGCTTTTCACATCGTCACTCCT
BDC strand on unused_m13mp18_53	GACAGGAACGGTACGCCAGAATCCTTTTTCACATCGTCACTCCT
BDC strand on unused_m13mp18_54	AACAGGAGGCCGATTAAAGGGATTTTTTTCACATCGTCACTCCT
BDC strand on unused_m13mp18_55	TCCTCGTTAGAATCAGAGCGGGAGCTTTTCACATCGTCACTCCT
BDC strand on unused_m13mp18_56	GCTTTGACGAGCACGTATAACGTGCTTTTCACATCGTCACTCCT
BDC strand on unused_m13mp18_57	CGCCGCTACAGGGCGCGTACTATGGTTTTCACATCGTCACTCCT
BDC strand on unused_m13mp18_58	TAACCACCACACCCGCCGCGCTTAATTTTCACATCGTCACTCCT
BDC strand on unused_m13mp18_59	TGGCAAGTGTAGCGGTCACGCTGCGTTTTCACATCGTCACTCCT
BDC strand on unused_m13mp18_60	AAGCGAAAGGAGCGGGCGCTAGGGCTTTTCACATCGTCACTCCT
BDC strand on unused_m13mp18_61	CGAACGTGGCGAGAAAGGAAGGGAATTTTCACATCGTCACTCCT
BDC strand on unused_m13mp18_62	GATTTAGAGCTTGACGGGGAAAGCCTTTTCACATCGTCACTCCT
BDC strand on unused_m13mp18_63	TAAATCGGAACCCTAAAGGGAGCCCTTTTCACATCGTCACTCCT
BDC strand on unused_m13mp18_64	TTTTGGGGTCGAGGTGCCGTAAAGCTTTTCACATCGTCACTCCT
BDC strand on unused_m13mp18_65	TACGTGAACCATCACCCAAATCAAGTTTTCACATCGTCACTCCT

T1R2F_HP	T1R2E_HP	T3R2F_HP	T3R2E_HP	T5R2F_HP	T5R2E_HP
T1R4F_HP	T1R4E_HP	T3R4F_HP	T3R4E_HP	T5R4F_HP	T5R4E_HP
T1R6F_HP	T1R6E_HP	T3R6F_HP	T3R6E_HP	T5R6F_HP	T5R6E_HP
T1R8F_HP	T1R8E_HP	T3R8F_HP	T3R8E_HP	T5R8F_HP	T5R8E_HP
T1R10F_HP	T1R10E_HP	T3R10F_HP	T3R10E_HP	T5R10F_HP	T5R10E_HP
T_1R12F_CYC_HP	T1R12E_CYC_HP	T3R12F_CYC_HP	T3R12E_CYC_HP	T5R12F_CYC_HP	T5R12E_CYC_HP

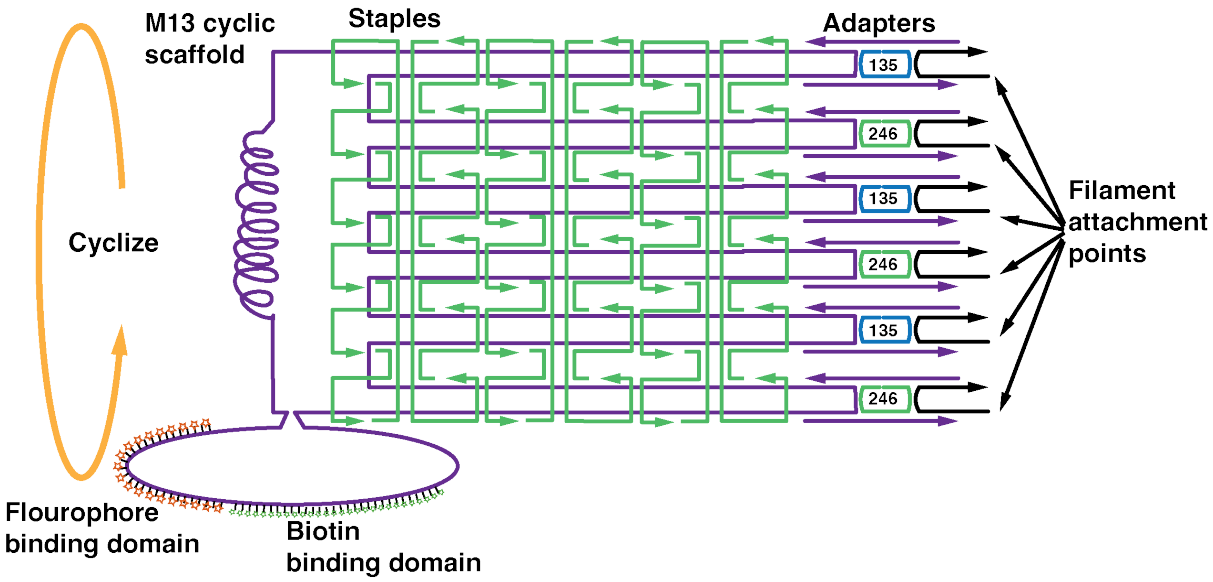

Figure S10. Seed staple array arrangement and spatial configuration
Seed design and protocols were adapted from previous work[1,2], and were used to develop the shorter variant of the origami-seed used through-out this work.

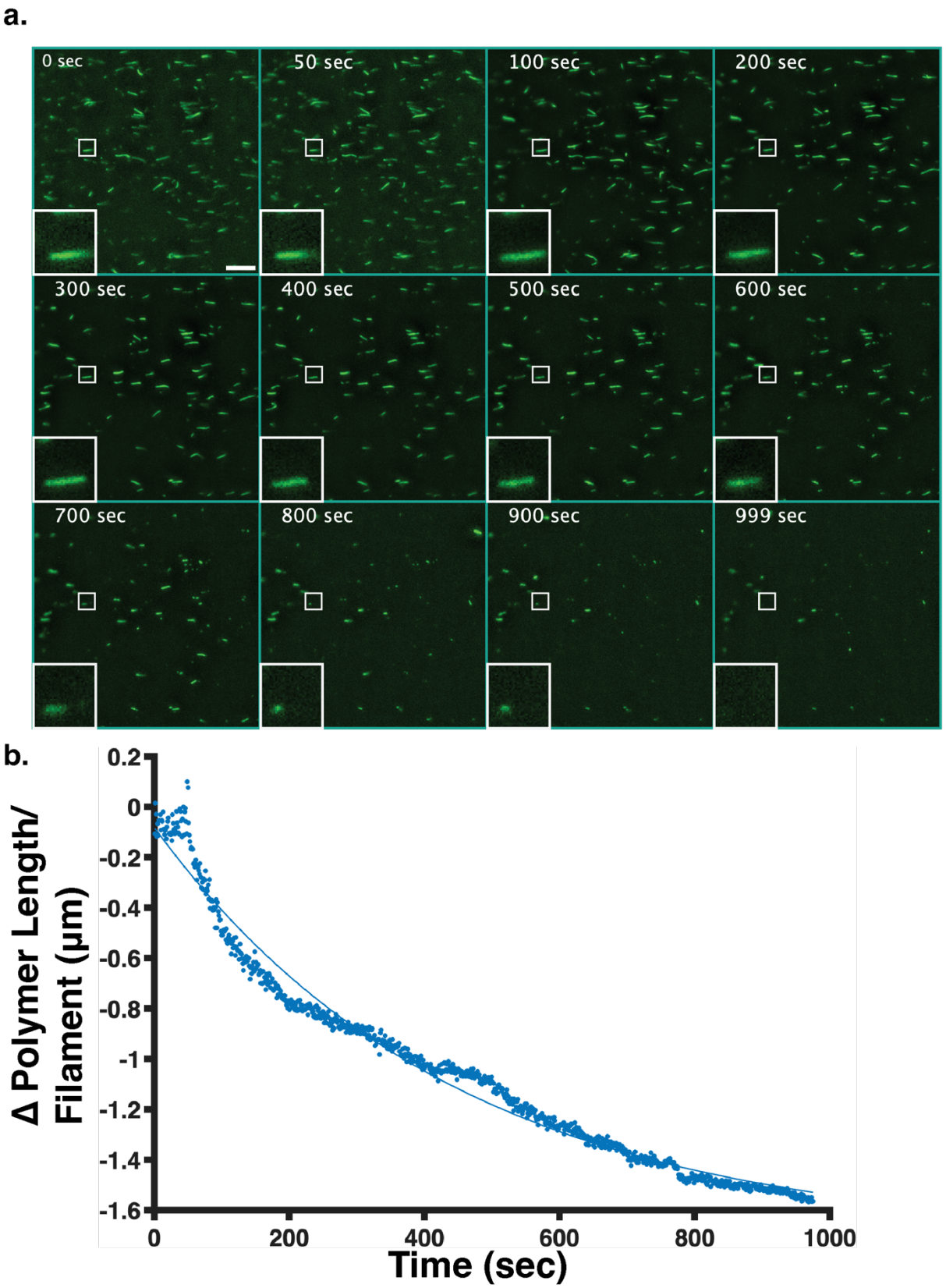

Figure S11. Polymer population dissolution in flow chamber as a result of switching MMCat/MMSc monomer-mix with buffer wash

a. Time series TIRF images depicting the gradual depolymerization and eventual depletion of the polymer population under a 3 μl/min flow of 1xTAE-Mg^{2+} buffer.

Origami seed channel was omitted for clarity, and can be viewed on Movie S6. **b.** Quantified time-dependent change in polymer length per filament.

a.

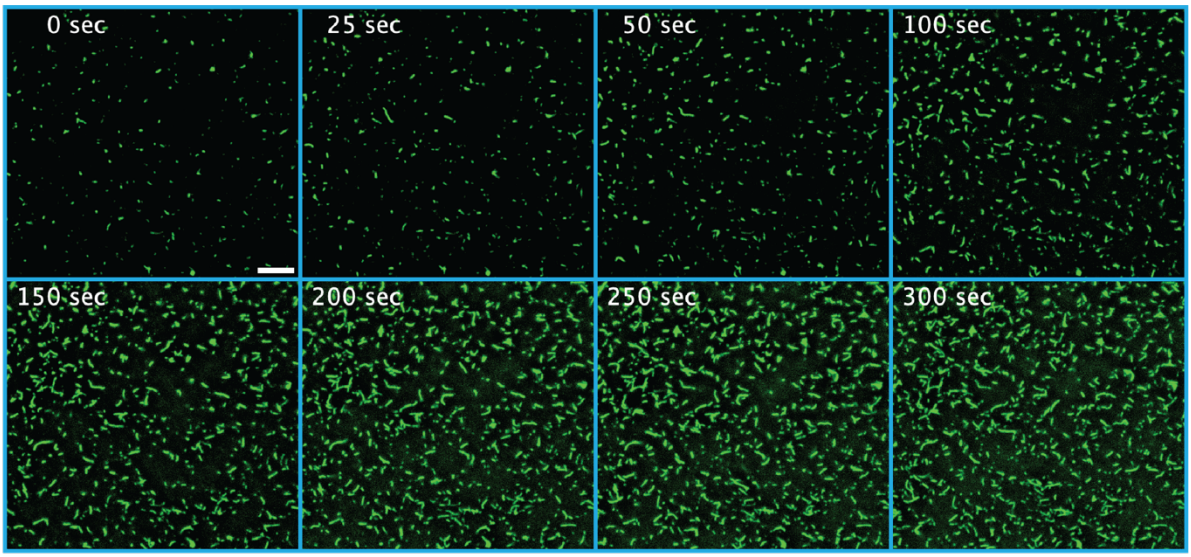

b.

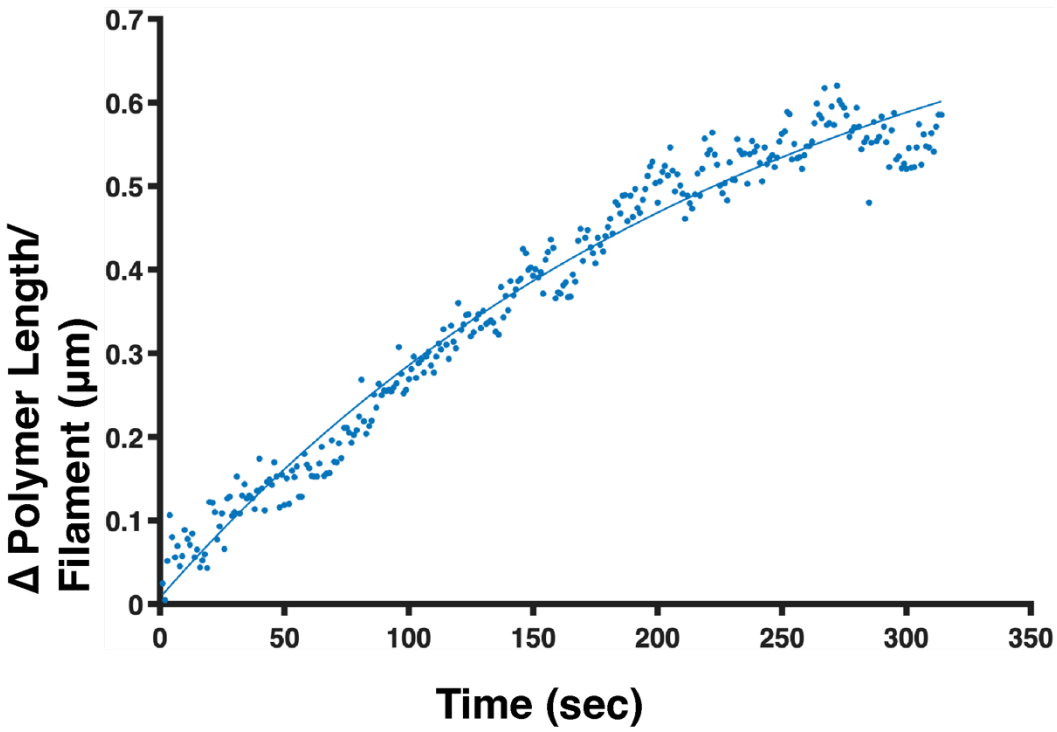

Figure S12. Polymer recovery in flow chamber

a. Time series TIRF images depicting the gradual polymer population recovery and eventual arrival to a new steady state of the polymer population under a 4±1 μl/min flow of 1xTAE-Mg^{2+} buffer. Origami seed channel was omitted for clarity, and can be viewed on Movie S7. **b.** Quantified time-dependent change in polymer length per filament.

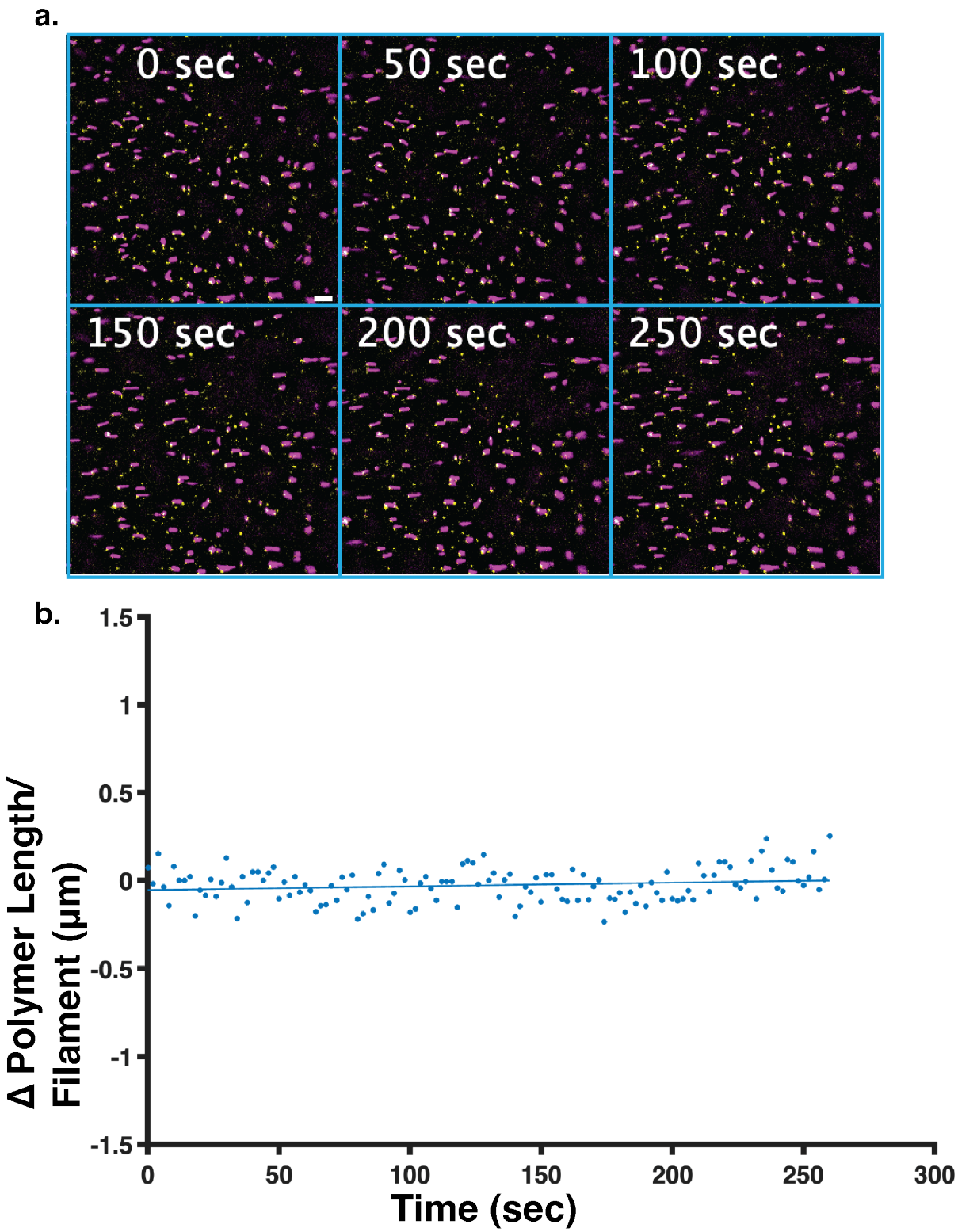

Figure S13. All DNA filament system with seed in flow chamber

a. Time series TIRF images demonstrating the depolymerization resistance of the all-DNA composed polymer system under a 5 μl/min flow of 1xTAE-Mg^{2+} buffer. Yellow: Origami seed, Magenta: all-DNA filaments. **b.** Quantified time-dependent change in polymer length per filament.

a.

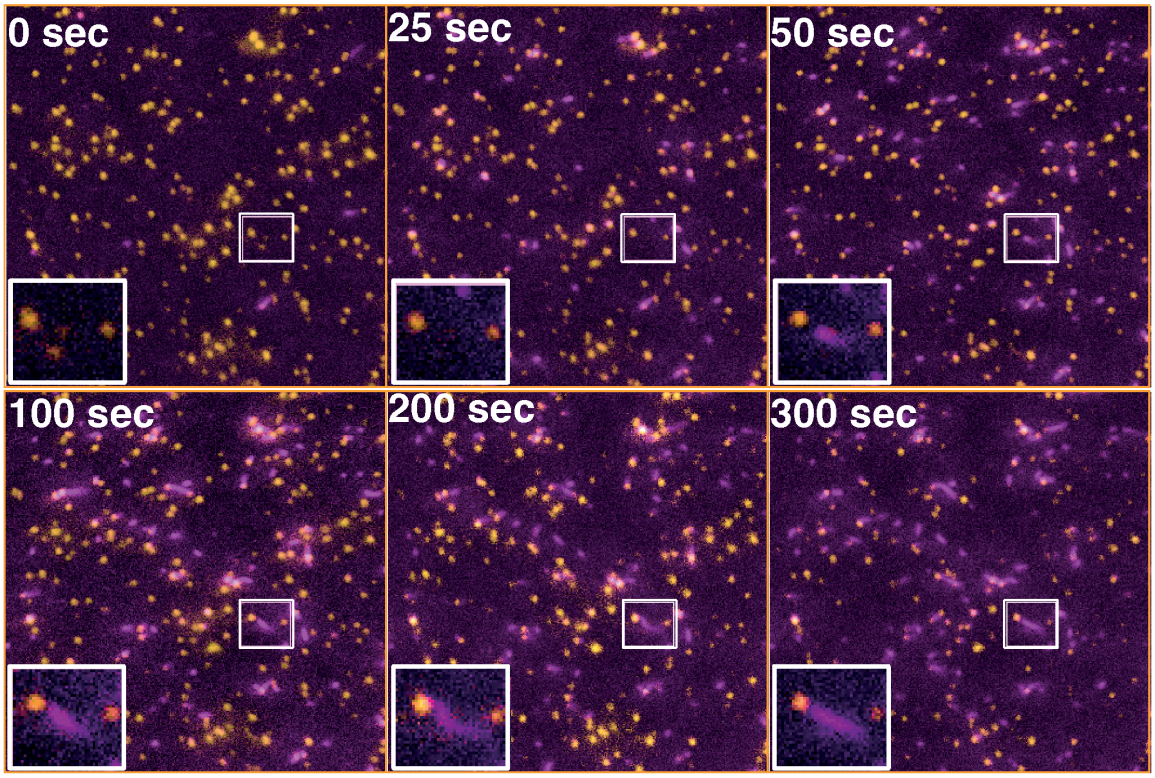

b.

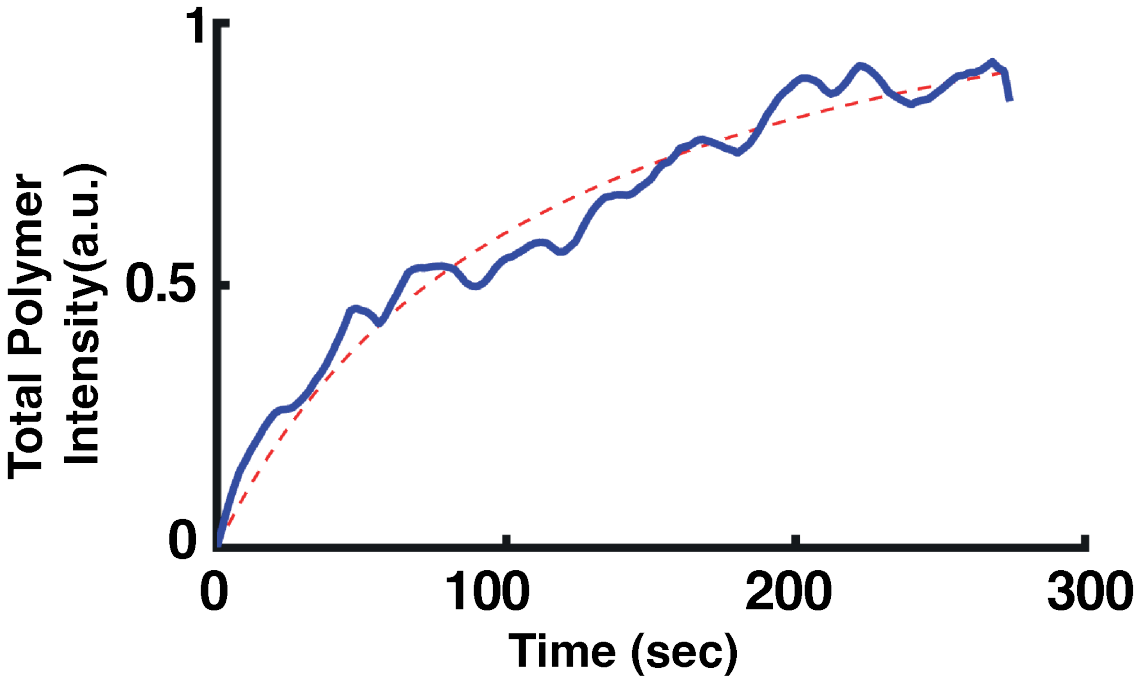

Figure S14. Filament evolution under flow of MMCat/MMSc and iDz

Time series TIRF images depicting the polymer population polymerizing under a multi-channel flow consisting of a 400nM MMCat/MMSc monomer mix, 3 µl/min, and 1.2 µM of the non-complementary catalyst iDz, 2 µl/min. **b.** Time-dependent change in total fluorescent intensity.

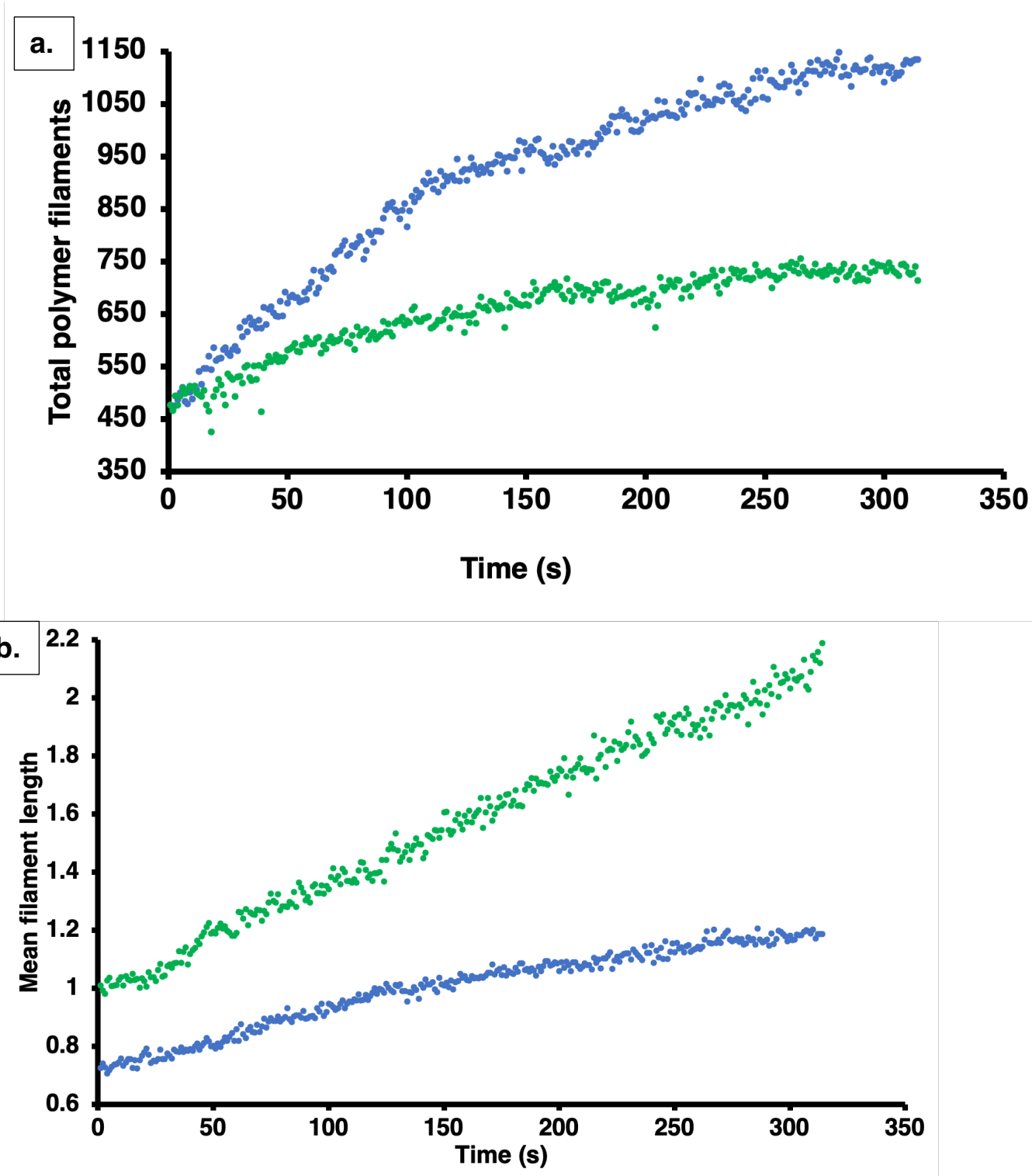

Figure S15. Comparison between +Cpl/+DzII and -Cpl/-DzII system parameters
a. Time dependent change in mean filament length for +Cpl/+DzII(green curve) and the -Cpl/-DzII(blue curve) system configurations. **b.** Time dependent change in number of total polymer filaments for the +Cpl/+DzII(green curve) and the -Cpl/-DzII(blue curve) system configurations.

References

1. Mohammed, A. M., Šulc, P., Zenk, J. & Schulman, R. Self-assembling DNA nanotubes to connect molecular landmarks. *Nature Nanotech* **12**, 312–316 (2017).
2. Jia, S. *et al.* Growth and site-specific organization of micron-scale biomolecular devices on living mammalian cells. *Nat Commun* **12**, 5729 (2021).
3. Schiffels, D., Liedl, T. & Fygenson, D. K. Nanoscale Structure and Microscale Stiffness of DNA Nanotubes. *ACS Nano* **7**, 6700–6710 (2013).